Impact of the Physicochemical Features of TiO2 Nanoparticles on Their In Vitro Toxicity

Ozge Kose, Maura Tomatis, Lara Leclerc, Naila-Besma Belblidia, Jean-François Hochepied, Francesco Turci, Jérémie Pourchez, Valérie Forest

Impact of the physicochemical features of TiO_2 nanoparticles on their *in vitro* toxicity

Ozge Kose[†], Maura Tomatis[‡], Lara Leclerc[†], Naila-Besma Belblidia[§,ǀ], Jean-François Hochepied[§,ǀ], Francesco Turci[‡], Jérémie Pourchez[†], Valérie Forest[†*]

[†]Mines Saint-Etienne, Univ Lyon, Univ Jean Monnet, INSERM, U 1059 Sainbiose, Centre CIS, F-42023 Saint-Etienne, France.

[‡]Dipartimento di Chimica and 'G. Scansetti' Interdepartmental Center for Studies on Asbestos and other Toxic Particulates, Università degli Studi di Torino, Torino, Italy

[§]Mines ParisTech, PSL Research University, MAT - Centre des matériaux, CNRS UMR 7633, BP 87 91003 Evry, France.

[ǀ] ENSTA ParisTech UCP, Institut Polytechnique Paris, 828 bd des Maréchaux, 91762 Palaiseau cedex France.

* **Corresponding author**: Valérie Forest:

Mines Saint-Etienne, 158 cours Fauriel, CS 62362, 42023 Saint-Etienne Cedex 2. FRANCE.

Email: vforest@emse.fr

Keywords

Titanium dioxide nanoparticles; cytotoxicity; pro-inflammatory response; reactive oxygen species; human lung cells.

Table of Content graphic

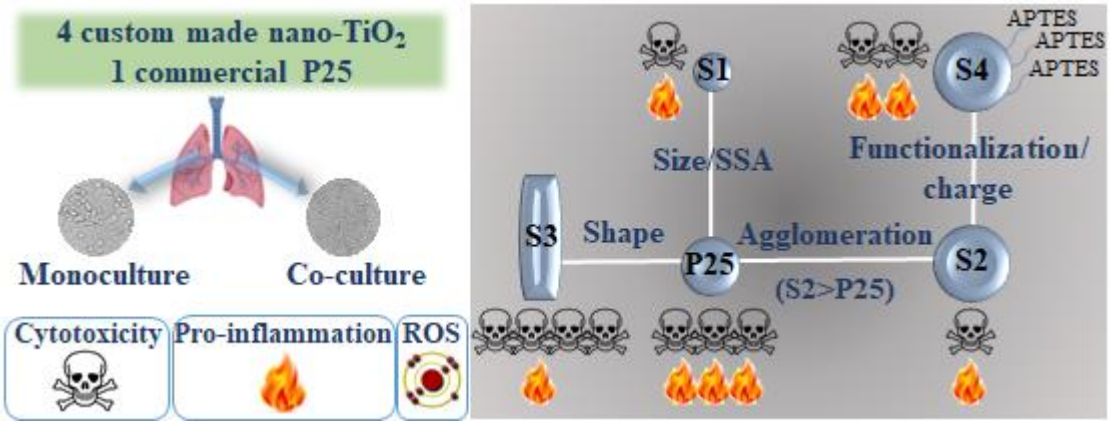

Abstract

The concern about titanium dioxide nanoparticles (TiO_2-NPs) toxicity and their possible harmful effects on human health has increased. Their biological impact is related to some key physicochemical properties, *i.e.* particle size, charge, crystallinity, shape, and agglomeration state. However, the understanding of the influence of such features on TiO_2-NP toxicity remains quite limited. In this study cytotoxicity, pro-inflammatory response, and oxidative stress caused by five types of TiO_2-NPs with different physicochemical properties were investigated on A549 cells used either as monoculture or in co-culture with macrophages differentiated from the human monocytic THP-1 cells. We tailored bulk and surface TiO_2 physicochemical properties and differentiate NPs for size/SSA, shape, agglomeration state, and surface functionalization/charge (APTES). An impact on the cytotoxicity and to a lesser extent on the pro-inflammatory responses depending on cell type was observed, namely: smaller, large-agglomerated TiO_2-NPs were shown to be less toxic than P25 whereas rod-shaped TiO_2-NPs were found to be more toxic. Besides, the positively-charged particle was slightly more toxic than the negatively-charged one. Contrarily, TiO_2-NPs, whatever their physicochemical properties, did not induce significant ROS production in both cell systems compared to non-treated control group. These results may contribute to better understanding of TiO_2-NPs toxicity in relation with their physicochemical features.

1. Introduction

Titanium dioxide (TiO_2) is an inorganic compound, which is widely used in a large range of industrial applications mainly due to its high refractive index or photocatalytic properties [1,2]. World production of TiO_2 nanoparticles (TiO_2-NPs) in 2014 was estimated to exceed 9 million metric tons [3] to be used in many consumer products such as paints (*e.g.* UV resistant and antibacterial self-cleaning paints), antiseptic-antimicrobial compositions, deodorization (purify/deodorize indoor air), inks, papers, plastics, UV-sunscreen, toothpastes, ceramics, and food products [3–5]. This makes TiO_2-NPs one of the most abundantly produced nanomaterials (NMs) showing various forms of shape, crystalline phases and nano size range. As it is the second most used NM in consumer products [6], the concern about TiO_2-NPs toxicity and their possible harmful effects on human health has increased [7–9].

The toxicity of NPs is greatly related to their interaction with biological systems. This interaction is associated with the physicochemical properties of the NPs [10]. Generally, cellular uptake of NPs is determined by their size, surface area, shape, surface charge, chemical composition, crystallographic phases and surface modifications [11]. The internalization of NPs through cell membrane might lead to potential hazards by interaction with intracellular biological macromolecules. It might cause an imbalance between cellular antioxidants and oxidants, in the favor of oxidants. As a result, the high accumulation of Reactive Oxygen Species (ROS) causes the oxidative stress. Oxidative stress responses are crucial for further pathological effects including genotoxicity, inflammation, and fibrosis. Previous studies have shown that relatively large surface areas/particle size have a critical role in increased incidence of lung injury and pulmonary inflammation [12,13]. Specifically, aerodynamic diameter of inhaled particles strongly influences particles deposition to occur in different regions of the human respiratory tract [14], and can cause different biological effects depending on the anatomic target of human respiratory tract (alveolar or tracheobronchial area) where they accumulate [15]. Studies

have also reported that the NP shape could affect toxicity during endocytosis or phagocytosis, *e.g.* the endocytosis of spherical NPs is a more favorable process than that of rod-shaped NPs [16,17]. Nonetheless, spherical NPs are usually less toxic than rod-shaped NPs [18–20].

Although there is growing scientific evidence about TiO_2-NPs toxicological and even pathological properties [21] the question of how the physicochemical features of TiO_2-NPs impact their *in vitro* toxicity has not yet been fully addressed, especially to foster a safer-by-design approach to NP production. Indeed, a safer-by-design approach aims at developing functional as well as safe nanomaterials from their conception, while current nanomaterials are regarded as intrinsically unsafe. The main objective of this approach is to know what property makes a nanomaterial or nanoproduct more or less safe [22]. Subsequent steps involve the application of this knowledge to industrial innovation processes; and as a result, NPs that are safer to human and environment are produced. The key factor in this regard is the comprehensive study of the toxicological effects of the physicochemical properties of NPs [23].

As TiO_2-NPs could be hazardous, for NP safety and for defining an adequate risk assessment, in particular to protect exposed workers and general population subjects, it is necessary to study how the physical and chemical properties of TiO_2-NPs determine their biological effects [24,25].

As one of the main exposure routes to these NPs is inhalation, in this study we aimed to determine the impact of physicochemical properties of TiO_2-NPs on their *in vitro* toxicity on human lung cell lines. A549 carcinoma epithelial cell line was used as a monoculture system. A co-culture system consisting of A549 and macrophages (differentiated from the human monocytic THP-1 cell line) was also used as an extended approach to reflect the interactions between different cell types in the lung after exposure to NPs. To that purpose, we thoroughly characterized five types of TiO_2-NPs with different and well-controlled physicochemical properties: a commercially available P25 sample and 4 custom-made TiO_2 samples. After

exposure, the cell response was assessed in terms of cell viability, pro-inflammatory response, and oxidative stress status.

2. Material and Methods

2.1 Physicochemical characterization of TiO_2 nanoparticles

In this study, we used five types of TiO_2-NPs with different and well-controlled physicochemical properties. In addition to P25 NPs (Evonik P25 CAS: 1317-70-0, Sigma-Aldrich, Saint-Quentin-Fallavier, France), used as a reference, four types of TiO_2-NPs samples differing in size, shape, agglomeration state and surface functionalization/charge were synthesized, they were named S1 to S4 as shown in Table 1.

Table 1. TiO_2-NPs used in this study with their specific characteristics.

S1	S2	S3	S4	P25
Custom-made for size/SSA	Custom-made for agglomeration	Custom-made for shape	Custom-made for functionalization/ charge	Commercial/ used as a reference

TiO_2-NPs were synthesized using Chen et al. [26] method. Basically, titanium (IV) butoxide (CAS: 5593-70-4 reagent grade 97%, Sigma-Aldrich, Saint-Quentin-Fallavier, France) was mixed with triethanolamine (CAS: 102-71-6, Analytical reagent 97%, VWR International, Fontenay-sous-Bois, France) in 1:2 molar ratio. The mixture was put in Teflon lined sealed autoclave and then heated at 150°C during 24 h. The pH values of the synthesis medium were adjusted using HCl or NH_4OH to tune particle size and morphology. Finally, the solutions were washed by three centrifugations using de-ionized water and the resulting products were dried in an oven at 40°C. Surface functionalization of S2 NPs was generated by aminopropyltriethoxysilane (APTES) using Zhao et al. [27] method. Briefly, 0.25 g of S2

nanopowder was dispersed in 25 mL de-ionized water by ultrasonication for 10 min. Then, the silane coupling agents APTES were added in the dispersion (molar ratio of 1:1). The mixture was sonicated until a clear solution was obtained and then refluxed at 80°C for 4h. After that, dispersed particles were separated from solvent by centrifugation (10 min at 1200 g) followed by washing with water at least 2 times. The final functionalized samples were then prepared in de-ionized water and labeled as S4. The features of NPs are reported in Fig. 1 and Table 2.

Stock suspensions of all NPs (1600 µg/mL) were prepared in de-ionized water (MilliQ systems, Millipore, Bedford, MA, USA) and sonicated with Branson Sonifier S-450 for 10 min at 89% amplitude. Before each physicochemical measurements and toxicity experiments stock suspensions were sonicated 15 min at bath sonicator and vortexed vigorously, fresh dilutions were prepared in low light conditions (*i.e.* 1 µW/cm^2 irradiation intensity) by using Dulbecco's Modified Eagle Medium (DMEM) to achieve the following final concentrations: 15, 30, 60 and 120 µg/mL. The pH of solutions was measured using a Metrohm digital pH meter of model 827.

The morphology and size distribution of NPs were analyzed by transmission electron microscopy (TEM) using a FEI TECNAI 20FST operating at 200 kV and scanning electron microscopy (SEM) at 2-3 kV on a Zeiss Sigma 300 microscope using a secondary electron (SE) detector. After each TEM image of each sample were chosen, the size distribution and the mean diameter were measured by ImageJ software. The hydrodynamic size and the agglomeration status of TiO_2-NPs (120 µg/mL) in de-ionized water and in DMEM were determined by using dynamic light scattering (DLS, Zetasizer Nano ZS Malvern Instruments, Worcestershire, UK) measurements. Surface charge of the NPs was monitored using electrophoretic light scattering (ELS, Zetasizer Nano ZS Malvern Instruments, Worcestershire, UK). Specific surface areas (SSA) were measured by linearizing the physisorption isotherm of

N_2 at 77 K with the classical method of Brunauer, Emmett and Teller (BET) (Volumetric Adsorption ASAP 2020, Micrometrics, USA) [28].

Raman spectroscopy (Horiba Jobin–Yvon Xplora spectrometer) and X-ray diffraction (XRD, Miniflex, Rigaku, Japan) techniques were used for the structural identification of the crystalline phases of NPs. Raman spectra were recorded on a system equipped with a confocal microscope and a nitrogen-cooled CCD detector. The high-resolution XRD patterns were measured in the continuous scan mode using a Step width of 0.05° (2θ). The scan range was 20–80°. Further parameters of the diffractometer were: Ni filtered K-beta radiation; voltage 40 kV; tube current 15 mA; scan speed 4° min^{-1}.

The spin trapping technique (5-5′- dimethyl-1-pirroline-N-oxide, DMPO, as trapping agent) associated to the electron spin resonance (ESR) spectroscopy (Miniscope 100 ESR spectrometer, Magnettech, Germany) was used to assess whether TiO_2-NPs have the potential to generate free radicals (hydroxyl, and carboxyl radical) under the same laboratory light conditions used for administration to cells. TiO_2 samples (120 µg/mL) were suspended in a buffered solution (potassium phosphate buffer 0.25 M, pH 7.4) containing 0.04 M DMPO or 0.04 M DMPO and 1 M sodium formate to detect hydroxyl and carboxyl radicals, respectively. The reaction mixtures were prepared under laboratory light conditions and then kept in the dark at 37°C. ESR spectra were recorded on aliquot (50 µl) withdrawn after 5, 10, 20 and 30 min of incubation. The instrument settings were as follows: microwave power 10 mW; modulation 1000 mG; scan range 120 G; center of field 3345 G. Blanks were performed with the same reaction mixtures without TiO_2. A suspension of P25, irradiated with a UV lamp for 30 minutes (100 W, 365 nm UV light, Cole-Parmer, Paris, France) was used as positive control. The irradiation intensity was 1 mW/cm^2 as measured by a radiometer (Model PCE-UV34, PCE Instruments UK Ltd, Southampton, UK). All experiments were repeated at least twice.

The presence of Al, Sb, Hg, Pb, Fe, Zn, As and Cd impurities in TiO_2 samples was determined by Agilent 7800 Inductively Coupled Plasma Mass Spectrometry (ICP-MS) as recommended by national and international standards (European Commission Directive 95/45/EC, Food and Drug Administration (FDA) Regulation 21-CFR, European Pharmacopoeia, Pharmacopoeia of the USA, etc.) that have set limiting values for the contents of these eight element impurities in TiO_2 samples [29].

2.2 Limulus Amebocyte Lysate (LAL) Assay: endotoxin contamination assessment

The amount of endotoxin present in the NP solutions was determined by the chromogenic method with ToxinSensor™ Chromogenic LAL Endotoxin Assay kit (Genscript, Piscataway, Associates of Cape CodInc, Falmouth, MA, USA) according to the manufacturer's instructions. All samples were prepared in endotoxin-free vials. The optical density was read at 545 nm. The amount of endotoxin in samples was calculated by comparison with a standard curve of endotoxin. Endotoxin concentrations were expressed as Endotoxin Units per milligram (EU/mg) of NPs.

2.3 Cell culture

The A549 human carcinoma epithelial cell line was supplied by the American Type Culture Collection (ATCC, CCL-185). The THP-1 human monocytic leukemia monocyte cell line (ATCC, TIB-202™) was a generous gift from Dr Ghislaine Lacroix from French National Institute for Industrial Environment and Risks (INERIS). A549 cells were used either as a monoculture or co-culture with macrophages differentiated from THP-1 cells (10 A549: 1 differentiated-THP-1 ratio).

A549 cells were grown in DMEM supplemented with 10% (v/v) fetal bovine serum (FBS, S1810; Biowest, Nuaillé, France), 1% penicillin-streptomycin (VWR International, Fontenay-

sous-Bois, France). A549 cells were grown in flasks and after reaching 80% confluency cells were trypsinized, washed with sterile Phosphate-Buffered Saline (PBS) and centrifuged at 1500 g for 10 min and subcultured. The flasks were stored at 37°C in a humidified atmosphere with 5% CO_2.

THP-1 was cultured in Roswell Park Memorial Institute (RPMI) 1640 (Gibco, Life Technologies, Cergy-Pontoise, France) containing 10% FBS and 1% penicillin-streptomycin. THP-1 cells were counted with Trypan Blue regularly and subcultured usually twice a week. Subcultures were started with a cell concentration of $2x10^5$ to $4x10^5$ viable cells/mL and cells were maintained at a concentration between 10^5-10^6 cells/mL in suspension. THP-1 cells were maintained in a humidified atmosphere containing 5% CO_2 at 37°C.

For the co-culture, THP-1 cells were differentiated into mature macrophage-like cells in 96-well plate with 30 ng/mL of Phorbol Myristate Acetate (PMA) (P1585, Sigma-Aldrich, Saint-Quentin-Fallavier, France) in RPMI for 24 h. After the incubation, cell surface was rinsed two times with DPBS. Then A549 cells were added on top of the differentiated THP-1 and the system was further cultivated for 24 h at a ratio of one differentiated THP-1 cell to ten A549 cells with direct cell-to-cell contact in DMEM supplemented with 10% (v/v) FBS and 1% penicillin-streptomycin.

2.4 Cell morphology

A549 cells and co-culture cells were seeded on 96 well plates ($1x10^5$ cells/well in 50 µL of medium) and were allowed to adhere for 24 h. After 24 hours exposure to the highest dose (120 µg/mL) of TiO_2 samples, supernatant was discarded and cell surfaces were washed with PBS. After cells were observed using optical microscopy (Leica ICC50 HD, Leica Microsystems, Nanterre, France) at 20 X magnification and pictures were captured.

2.5 Determination of cell viability

Cell viability was determined by Trypan blue exclusion since TiO_2-NPs have been reported to has interactions with MTT, XTT and LDH viability assays [30,31]. Trypan blue is a cell membrane-impermeable azo dye that live cells exclude whereas dead cells do not. $1.5x10^6$ cells/well were plated onto 6-well microtiter plates in 1000 µL culture medium with or without TiO_2-NPs. After incubation for 24 h at 37°C in a humidified incubator, the culture medium was removed, cells were washed with PBS and trypsinized. 20 µL cell suspensions were mixed with 80 µL Trypan blue dye to obtain 1:5 dilution and cells were counted under the microscope using Thoma cell counting chamber. Results are expressed as the mean of three independent experiments and relative to control (unexposed) cells.

2.6 Pro-inflammatory response

A549 cells and co-culture cells were seeded in 96-well-plates ($1x10^5$ cells/well in 50 µL of medium) and were allowed to adhere for 24 h. NPs were diluted in DMEM cell culture medium to reach the following final concentrations: 15, 30, 60 and 120 µg/mL. After 24h cell exposure to TiO_2-NPs, the production of Tumor Necrosis Factor alpha (TNF-α) was evaluated in co-culture using a commercial ELISA Kit (Quantikine® Human TNF-α Immunoassay; R&D Systems, Lille, France) according to the manufacturer's instructions. Interleukin-8 (IL-8) production was assessed in the two cell systems (A549 cells and A549/ differentiated-THP-1 co-culture) after exposure to TiO_2-NPs for 24 h by a commercially available ELISA kit (Quantikine® Human IL-8 Immunoassay; R&D Systems, Lille, France) according to the manufacturer's instructions. The optical density of each sample was determined using a microplate reader (Multiskan RC; Thermolabsystems, Helsinki, Finland) set to 450 nm. Three independent experiments were performed, the production of TNF-α and IL-8 were reported to that of control (unexposed) cells.

2.7 Determination of Reactive Oxygen Species (ROS) production

A549 cells and co-culture cells were seeded in 96 well black polystyrene microplates ($1x10^5$ cells/well in 50 μL of medium) and were allowed to adhere for 24 h before assay. After 90 min and 24 hours exposure to 15, 30, 60 and 120 μg/mL TiO_2-NPs, the level of ROS was determined using the OxiSelect™ kit from Cell Bio Labs (San Diego, CA, USA) according to the manufacturer's instructions. Fluorescence was detected using a Fluoroskan Ascent fluorometer (Excitation: 480 nm, Emission: 530 nm, Thermolabsystems), and the generation of ROS was reported to that control (unexposed) cells.

2.8 Statistical analyses

Statistical analyses were performed using GraphPad Prism® (version 8.0, GraphPad Software, San Diego, CA, USA). All data were presented as mean ± standard error of the mean (SEM). Differences were considered to be statistically significant when *P* value was less than 0.05. One-way Anova Tukey test analysis was performed for comparison between control and experimental groups and among experimental groups.

3. Results

3.1 Physicochemical features of TiO_2 nanoparticles

The physicochemical characterization of five different TiO_2-NPs was performed using TEM, SEM, DLS, BET, ζ-potential, Raman spectroscopy, XRD and ICP-MS to provide clear insight into their primary size, hydrodynamic size, shape, specific surface area, surface charge, crystallinity and chemical composition. The key toxicity-relevant features of the TiO_2-NPs are listed in Table 2 with corresponding TEM images shown in Fig 1.

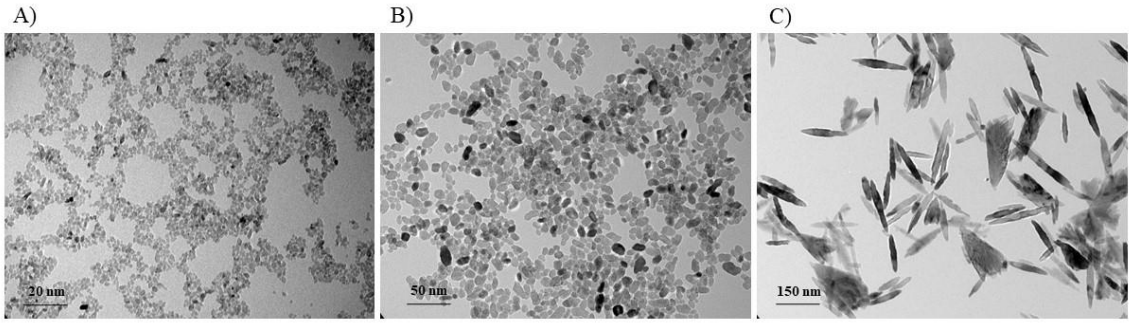

Fig. 1. Transmission electron microscope images of TiO_2-NPs (A) S1, (B) S2, (C) S3.

Please note that TEM images were shown to illustrate the NP shape, and as surface functionalization is not expected to alter the NP shape, we consider that TEM picture of S2 is representative of that of S4.

Table 2. Particle primary size, specific surface area (SSA), shape, average hydrodynamic size, polydispersity index (PDI) and zeta potential in culture media (in DMEM) and in de-ionized water (D.I. H_2O) after dispersion of TiO_2-NPs (120µg/mL). All data are presented as mean of three independent characterizations ± SD. [a] Dynamic light scattering (DLS) measurements are the mean of at least 3 runs each containing 20 sub-measurements. [b] Polydispersity index. SSA: specific surface area, FBS: Fetal bovine serum. [*]minimum Feret diameter, [§] maximum Feret diameter.

				D.I. H_2O			**DMEM + 10%FBS**		
	Primary size (nm)	**SSA (m^2/g)**	**Shape**	**Average hydrodynamic size[a] (nm)**	**PDI [b]**	**Zeta potential (mV) pH 7.5**	**Average hydrodynamic size[a] (nm)**	**PDI [b]**	**Zeta potential (mV) pH 7.5**
S1	15	146	Spherical	211.4 ± 2.3	0.145 ± 0.01	-13.2 ± 4.2	226 ± 9.1	0.282±0.01	-33.8 ± 1.8
S2	30	61	Spherical	969.3 ± 39.5	0.266 ± 0.01	-13.8 ± 4.4	1094 ± 46.4	0.364 ± 0.04	-32.6 ± 1.7

S3	20* - 250§	41	Rod	1419 ± 16.6	0.405 ± 0.08	-15.8 ±4.0	1275 ± 66.6	0.179±0.02	-33.7 ± 3.5
S4	30	61	Spherical	1049 ±146.3	0.823± 0.13	12.3 ± 0.5	1398 ± 54.9	0.475± 0.01	-36.4 ± 3.5
P25	21	55	Spherical	256.4 ± 136.6	0.272± 0.02	-15.2 ± 5.3	325 ± 4.1	0.260±0.01	-33.1 ± 1.7

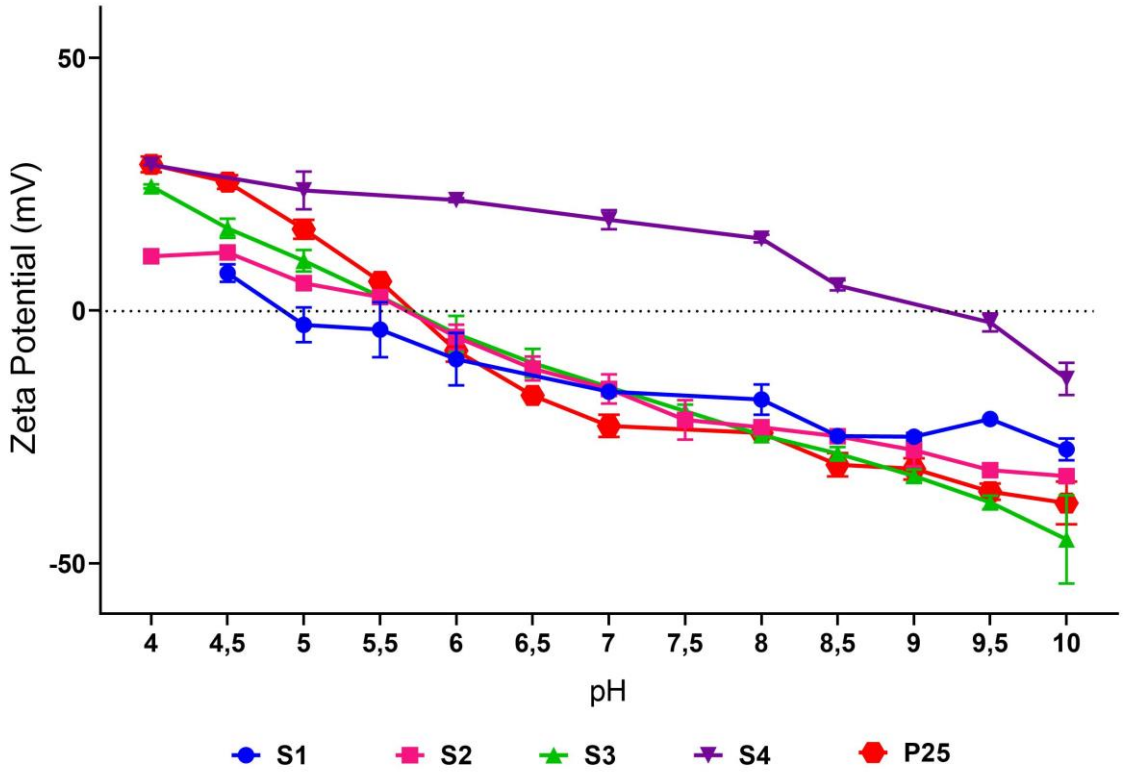

Fig. 2. The zeta potential vs. pH curves of TiO_2-NPs in 1 mM sodium nitrate ($NaNO_3$) solution. Values are the mean ± SEM of three independent experiments.

All samples exhibited a negative surface charge up to pH < 5.5, while S4 surface was positively charged in almost all pH values investigate (pH < 9.5) (Fig. 2). S4 differentiated from the other samples also in D.I. H_2O at pH 7.5, exhibiting a remarkably positive surface charge (Table 2) which is due to the presence of amine groups ($-NH_2$) on the surface of the NPs after APTES modification. In the culture medium (pH 7.5), all samples, including S4, exhibited a negative surface charge. The opposite sign of the surface charge of S4 in D.I. H_2O and DMEM may be

due to the different adsorption and affinity of protons on the surface of the particle in the culture medium.

Raman spectra and XRD pattern (Supporting information) of TiO_2-NPs confirmed the anatase phase of S1-S4 and anatase-rutile mixed phase (ca. 90:10) of P25.

The free radical generation of TiO_2-NPs is shown in Fig. 3. No ESR spectra of the DMPO-$HO^{\bullet}$ and of the DMPO-$CO_2^{\bullet-}$ adducts were observed for the TiO_2 samples under the same light conditions used in the cellular tests, thus suggesting that the photocatalytic activity of TiO_2-NPs is not a parameter that may affect toxicity results in this study.

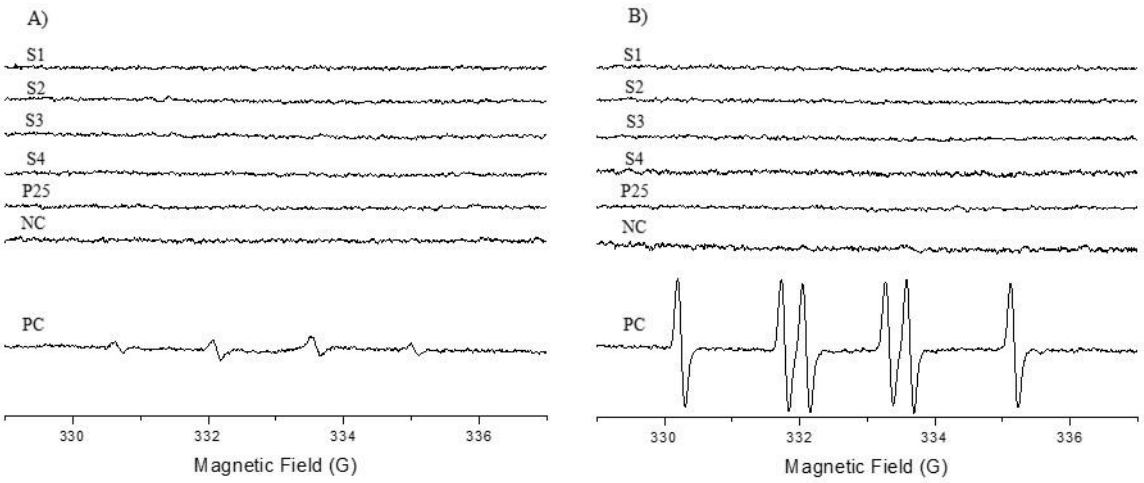

Fig. 3. Generation of $HO^{\bullet}$ (A) and $CO_2^{\bullet-}$ (B) radicals. Negative Control (NC) corresponds to buffer solution without particles. Positive Control (PC) corresponds to UV-irradiated P25. The number of radicals produced is proportional to the intensity of the ESR signal.

The trace toxic impurities of Cd, Hg, As, Pb, Sb and Zn in the tested samples met purity requirements of typical maximum tolerable limits of 0.5, 0.5, 3, 10, 50 and 50 mg/kg, respectively. Moreover, all particle samples were tested by endotoxin assay for the possible presence of endotoxin. Endotoxin content was found to be below the detection limit for all the

samples. Since the tested NPs did not contain toxic elements and endotoxins, it could be claimed that, the possible toxic effects after NP exposure are only caused by TiO_2-NPs themselves.

3.2 Cell morphology

Fig. 4 and Fig. 5 illustrate the morphology of A549 cells and A549/ differentiated-THP-1 co-cultured cells after 24 h exposure to the highest dose of TiO_2-NPs (120 µg/mL), respectively.

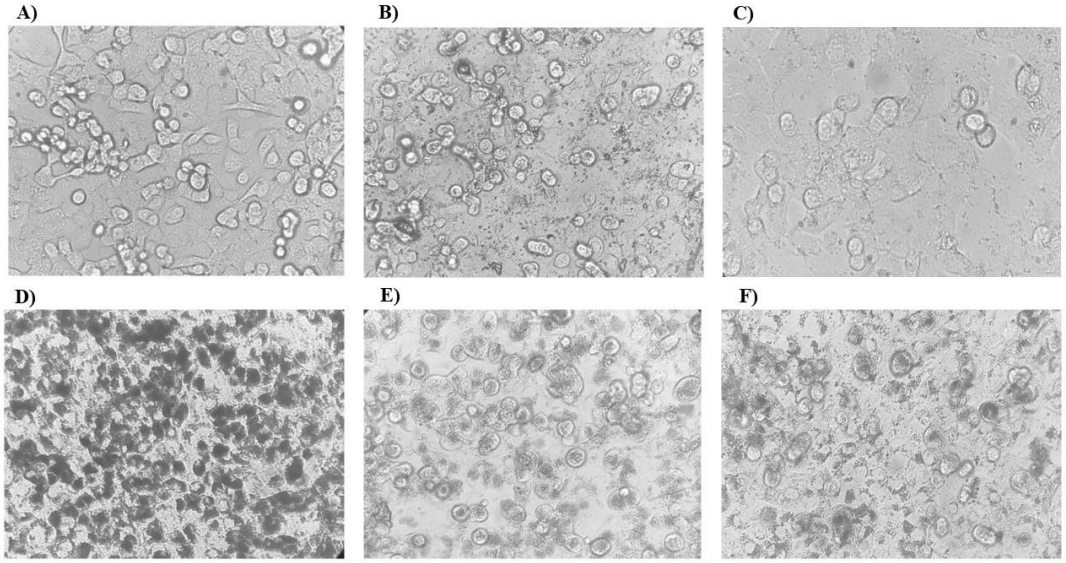

Fig. 4. Microscopic images of A549 cells exposed to 120 µg/mL TiO_2-NPs for 24 h (20 X magnification). A) Control cells (unexposed to NPs), B) S1, C) S2, D) S3, E) S4, F) P25.

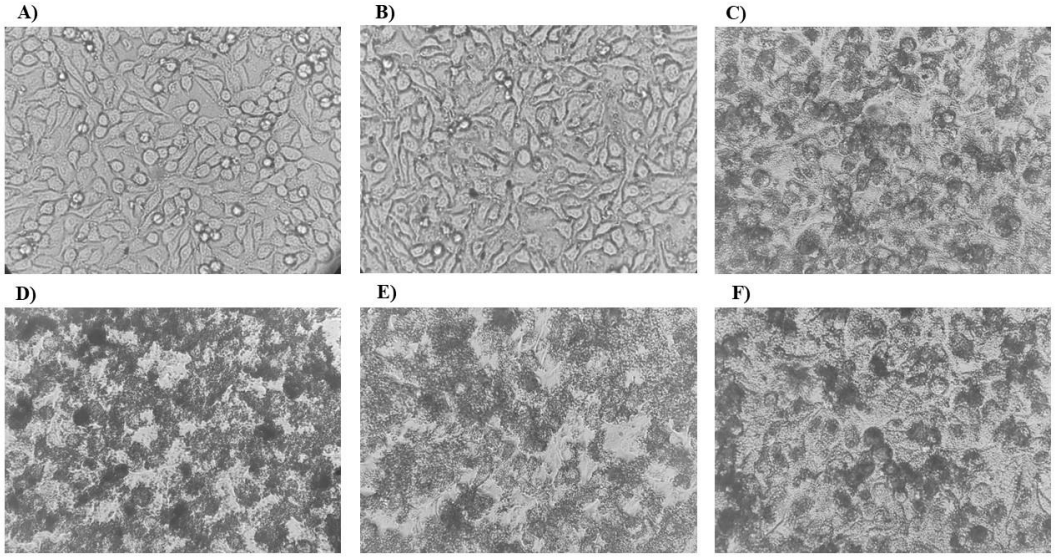

Fig. 5. Microscopic images of co-culture cells exposed to 120 µg/mL TiO_2-NPs for 24 h (20X magnification). A) Control cells (unexposed to NPs), B) S1, C) S2, D) S3, E) S4, F) P25.

Please note that we chose the highest NP concentration (120 µg/mL) to illustrate the cell morphological changes induced as they were more pronounced in this condition. However, cell morphology alterations were not the same depending on the NP concentration and type. For instance, with the smallest NP concentration, cell morphology was similar to that of control cells. Although such changes should deserve further investigation, here our primary goal was to verify that the cell viability assessment was consistent with cell morphology observations.

3.3 Cell viability

Cell viability, assessed by Trypan Blue, after exposure to TiO_2-NPs of A549 cells and A549/ differentiated-THP-1 co-culture is reported in Fig. 6 and 7, respectively.

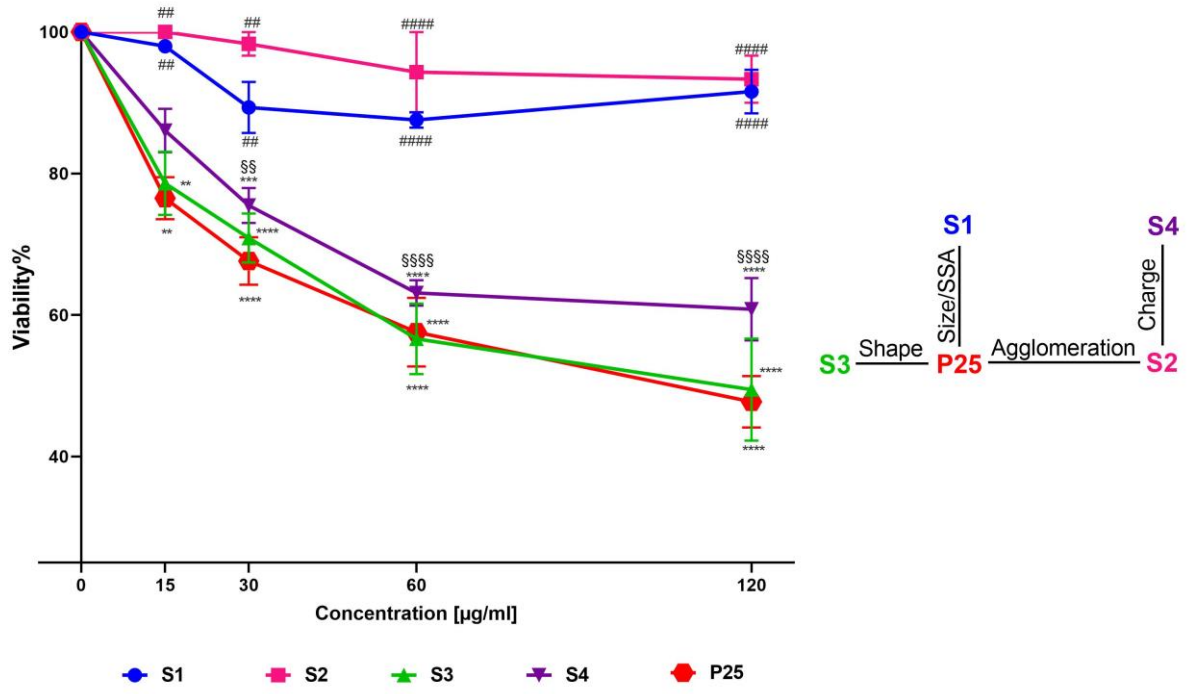

Fig. 6. Cell viability assessed by Trypan Blue assay 24 h after A549 cells were exposed to TiO_2-NPs at the indicated concentrations. Values are the mean ± SEM of three independent experiments. Statistically different from control (∗∗) $P < 0.01$, (∗∗∗∗) $P < 0.0001$. Statistically different from P25 (##) $P < 0.01$, (####) $P < 0.0001$. Statistical difference between S2 and S4 (§§) $P < 0.01$, (§§§§) $P < 0.0001$. Statistical analyses were conducted using one-way Anova analyses, followed by Tukey's multiple comparison test.

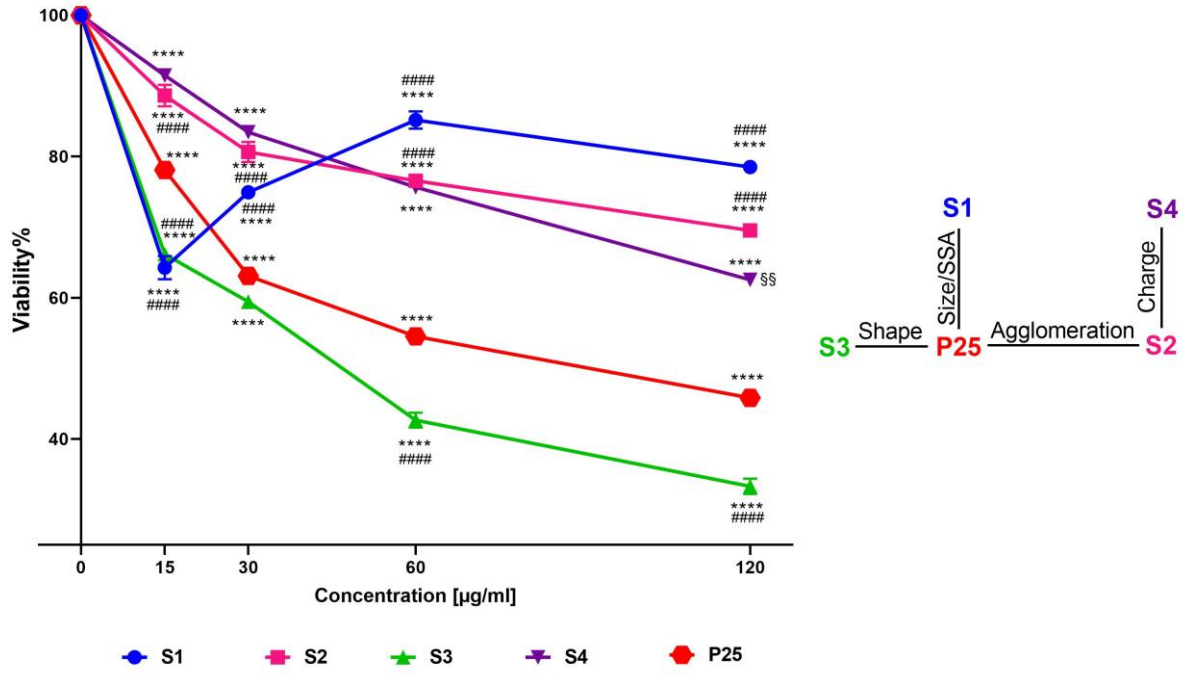

Fig. 7. Cell viability assessed by Trypan Blue assay 24 h after co-culture cells were exposed to TiO_2-NPs at the indicated concentrations. Values are the mean ± SEM of three independent experiments. Samples statistically different from control (∗∗∗∗) $P < 0.0001$. Statistically different from P25 (####) $P < 0.0001$. Statistical difference between S2 and S4 (§§) $P < 0.01$. Statistical analyses were conducted using one-way Anova analyses, followed by Tukey's multiple comparison test.

In general, a decrease in cell viability was observed after incubating A549 cells with all TiO_2-NPs although not statistically significant for S1 and S2. Statistically significant differences were found between P25 and S1, P25 and S2, S2 and S4.

The co-culture system is considered a more sensitive model than monocultures and better reflect the real tissue environment [32–34]. In co-culture, the tested NPs caused slightly more cell loss than in the A549 cell monoculture. The cell viability decreased in a dose-dependent manner in all samples except S1 (Fig. 7). The drastic drop of cell viability at the lowest S1 concentration is quite peculiar. We assume it might be due to experimental artifacts. Direct interaction between NPs and test reagents might cause artifacts however there is no evidence that Trypan blue interacts with TiO_2 unlike MTT, and LDH viability tests. Furthermore, artifacts may be a result of unacknowledged impurity (*e.g.* metal) or endotoxin contamination leading to an overestimation of NP toxicity, however we assessed toxic element impurity and endotoxin levels and did not observe any contamination. Other possible causes for artifacts include unexpected changes to 15 µg/mL S1 NPs (dissolution, agglomeration, oxidation, etc.) during sample preparation (ultrasonication may cause multiple undesirable and hard to quantify changes), or during testing (settling, dissolution, agglomeration, etc.) leading to inaccurate dosing. It is hard to definitively determine the sources of artifacts and further testing with regard to this aspect is necessary.

The exposure to S3 and P25 induced a higher cell viability loss than S1, S2 and S4. The maximal cell loss was observed for S3. Statistically significant differences were observed when comparing P25 to S1, P25 to S2 and P25 to S3 ($P < 0.0001$, all). When comparing S2 to S4, statistically significant difference was observed only at the highest dose (120 µg/mL, $P < 0.01$).

3.4 Pro-inflammatory response

As IL-8 is a major pro-inflammatory mediator in A549 cells and TNF-α is a pro-inflammatory cytokine secreted from monocytes/macrophages, IL-8 was assessed for A549 and IL-8 and TNF-α were assessed for the co-cultures. Results are reported in Fig. 8, and Fig. 9.

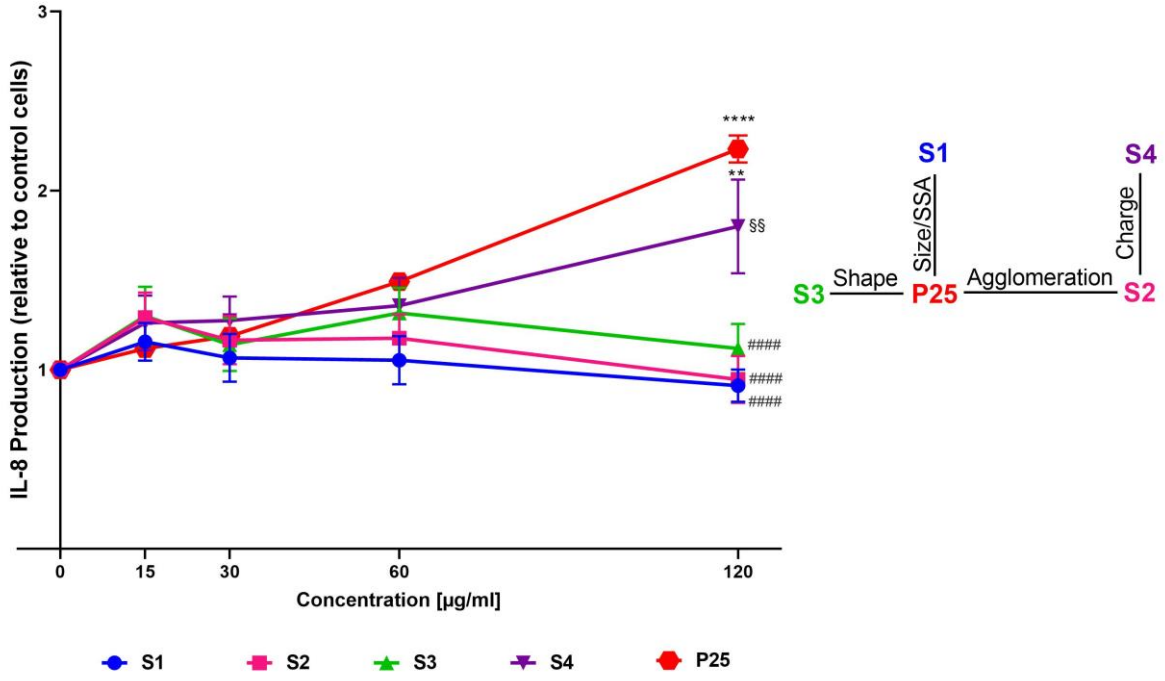

Fig. 8. IL-8 production after 24 h exposure to the indicated concentrations of TiO_2-NPs in A549 cells. Values are the mean ± SEM of three independent experiments. Statistically different from control (∗∗) $P < 0.01$, (∗∗∗∗) $P < 0.0001$. Statistically different from P25 (####) $P < 0.0001$. Statistical difference between S2 and S4 (§§) $P < 0.01$. Statistical analyses were conducted using one-way Anova analyses, followed by Tukey's multiple comparison test.

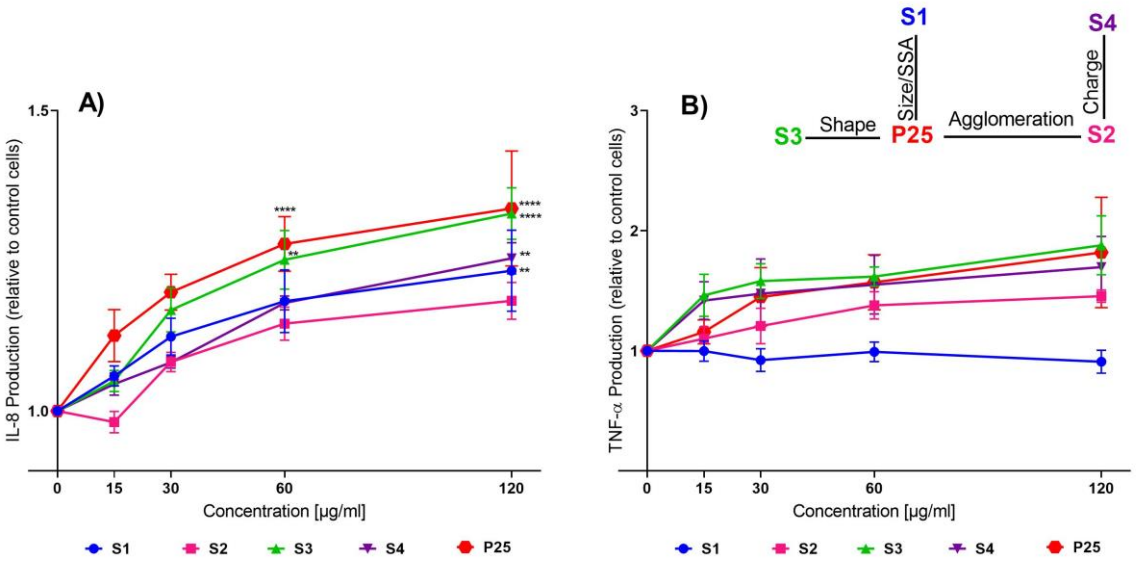

Fig. 9. IL-8 (A) and TNF-α (B) production after 24h exposure to the indicated concentrations of TiO_2-NPs in co-culture cells. Values are the mean ± SEM of three independent experiments. Statistically different from control (∗∗) $P < 0.01$, and (∗∗∗∗) $P < 0.001$. Statistical analyses were conducted using one-way Anova analyses, followed by Tukey's multiple comparison test.

In A549 cells, S4 and P25 samples caused a dose-dependent increase in IL-8 production compared to the control group and showed a statistically significant difference at the highest concentration (S4, $P< 0.01$; P25, $P< 0.0001$). When comparing P25 to S1, S2, and S3 only the highest NP concentration (120 µg/mL) induced significant productions of IL-8 ($P< 0.0001$, all). When comparing S2 to S4, statistically significant difference was observed only at the highest dose (120 µg/mL, $P < 0.01$).

In co-culture, all samples caused a dose-dependent increase in IL-8 production compared to the control group although not statistically significant for S2. When IL-8 production was compared between P25 and the other samples, no statistically significant difference was found.

Except S1, all groups showed concentration-dependent increase in TNF-α production although not statistically significant. When compared with P25, no statistically significant difference was found.

3.5 Reactive oxygen species (ROS) production

Fig. 10 and Fig. 11 report ROS production after exposure to the different TiO_2-NPs of A549 cells and A549/ differentiated-THP-1 co-culture respectively.

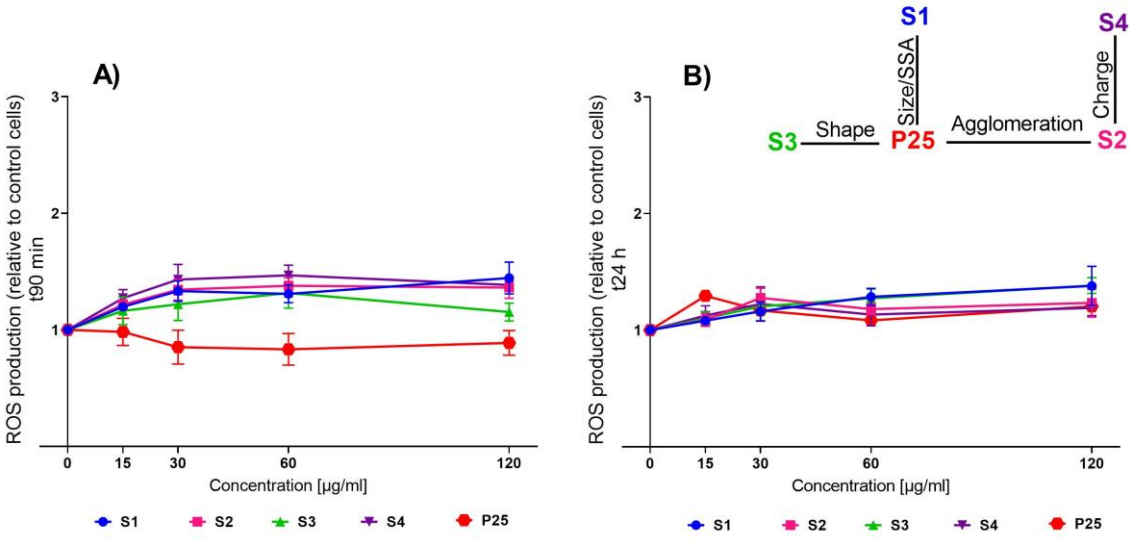

Fig. 10. ROS production after 90 min (A) and 24 hours (B) exposure to the indicated concentrations of TiO_2-NPs in A549 cells. Statistical analyses were conducted using one-way Anova analyses, followed by Tukey's multiple comparison test.

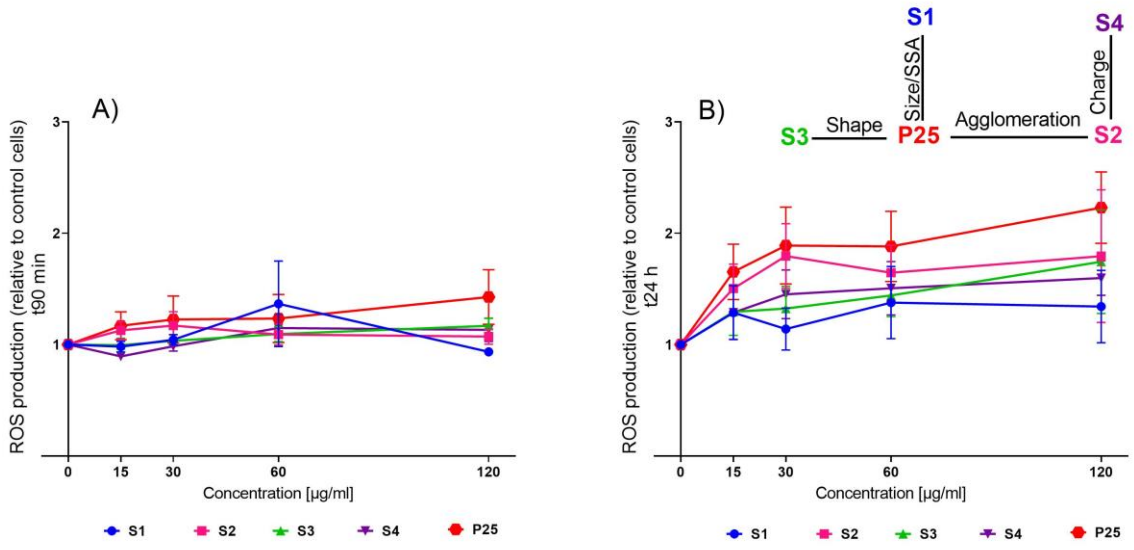

Fig. 11. ROS production after 90 min (A) and 24 hours (B) exposure to the indicated concentrations of TiO_2-NPs in co-culture. Statistical analyses were conducted using one-way Anova analyses, followed by Tukey's multiple comparison test.

TiO_2-NPs did not induce significant ROS production neither in A549 cells nor in co-culture compared to the control group (unexposed to TiO_2-NPs) whatever the time of analysis (90 min or 24 h).

4. Discussion

As it is commonly acknowledged that the physicochemical properties of NPs (*e.g.* size, shape, solubility, aggregation, etc.) strongly influence their toxicity, we aimed to determine the impact of such features on TiO_2-NPs toxicity on human lung cell lines. As illustrated by Fig. 12 and based on the physicochemical features of the different NPs, by comparing P25 and S1 we were able to highlight the impact of size and SSA on TiO_2-NPs cytotoxicity. We compared S2 and P25 to investigate the effect of agglomeration on toxicity as this feature was different between these samples, whereas their primary size, specific surface area, surface charge, and shape were all similar. The influence of particle shape was investigated by comparing rod-shaped S3 with

isometric P25 that share similar specific surface areas. Lastly, the surface charge impact on cell response was compared between S2 and S4. It is important to state that the crystalline phase of synthesized NPs and P25 are different from each other in this study. P25 is a mixture of anatase and rutile (approximately 90% anatase and 10% rutile), while other samples have a pure anatase structure. Several studies have shown that anatase is more toxic than similarly sized rutile TiO_2-NPs [35–37]. Therefore, we can confidently affirm that the anatase phase might be more responsible than the rutile phase for the toxic manifestations that P25 may create. A summary of our observations is reported in Table 3.

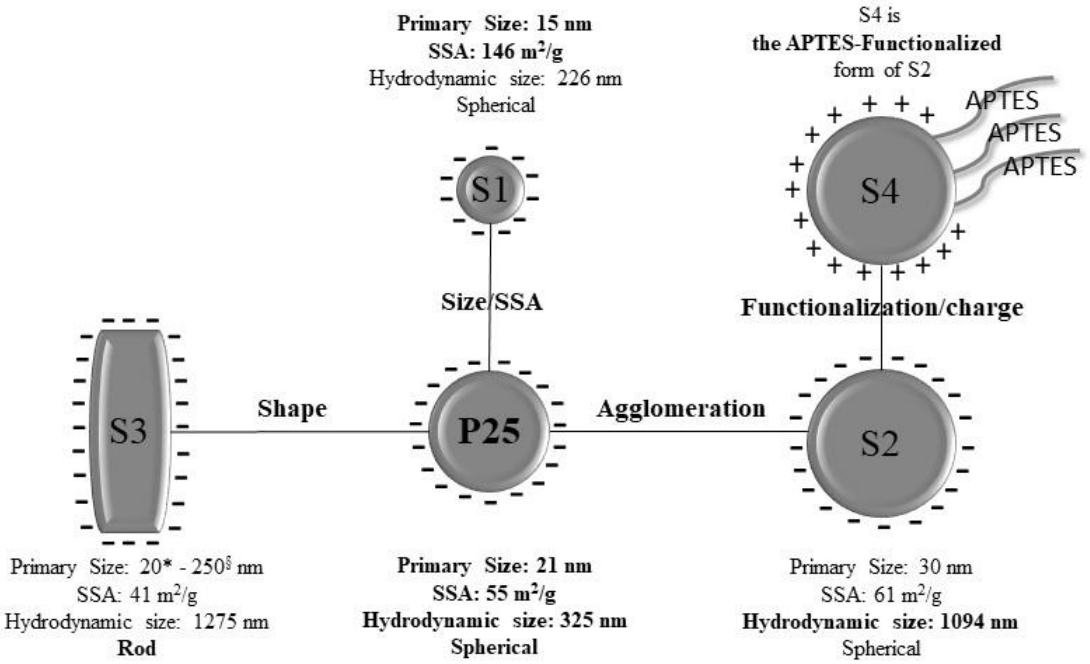

Fig. 12. Comparison of NPs with regard to their primary size/SSA, shape, agglomeration state, and surface functionalization/charge (APTES). Particle properties that differ from P25 TiO_2 are reported in bold. (-) indicate negative surface charge, (+) indicate positive surface charge, *minimum Feret diameter, § maximum Feret diameter.

Table 3. Impact of TiO_2-NPs size and SSA, shape, agglomeration state and functionalization on their cytotoxicity. + and – indicate an impact or no impact of the physicochemical features on the cytotoxicity respectively.

Impact of the indicated physicochemical features on cytotoxicity as evaluated by comparison between the indicated samples		Cell viability		Pro-inflammatory effect		Oxidative stress	
		A549	A549/ differentiated-THP-1	A549	A549/ differentiated-THP-1	A549	A549/ differentiated-THP-1
Size&SSA	P25 vs S1	+	+	(+ only at the highest dose)	-	-	-
Shape	P25 vs S3	-	+	(+ only at the highest dose)	-	-	-
Agglomeration	P25 vs S2	+	+	(+ only at the highest dose)	-	-	-
Surface charge	S2 vs S4	+	(+ only at the highest dose)	-	-	-	-

As highlighted in the introduction, a safer-by-design approach cannot be achieved without knowing the impact of physicochemical properties of NPs on their toxicity. In R&D phase of the safer-by-design approach, the assessment of the hazard profile of NPs exhibiting different physicochemical properties is the first step for avoiding their adverse effects [38]. The results obtained in this study (as summarized in Table 3 and further discussed below) provide data for the design and development of safer TiO_2-NPs.

4.1. Size and surface area effects

To determine the effects of the size and surface area of the TiO_2-NPs on their cytotoxicity, we compared S1 and P25 NPs, whose agglomeration states in the culture medium were very similar.

Generally, P25 (21 nm) caused more cell death than smaller sized S1 (15 nm). This finding is consistent with observations at the microscope of cell morphology. Cells were more affected when incubated with P25. P25 also induced a higher IL-8 production in A549 than S1 at the highest NP concentration. Finally, ROS production was similar between P25 and S1. These findings suggest a NP size and surface area impact on cell viability and pro-inflammatory response, but only at the highest NP concentration. Our findings are consistent with studies

showing that size and surface area of NPs might contribute to cytotoxicity [39,40]. In agreement with our finding that larger particles caused more toxicity, Park et al. [18] showed that 1 μm TiO_2-Degussa microparticles caused more pronounced morphological changes than smaller 30 nm TiO_2-NPs in A549 cells. Another study [41] reported that mouse neuroblastoma (Neuro-2A) cells showed much lower cell viability when incubated with 150 nm nickel ferrite NPs than with 10 nm particles. Pan et al. [42] reported that 1.4 nm sized gold NPs caused more cytotoxicity than 1.2 nm and 0.8 nm gold NPs on the HeLa cervix carcinoma epithelial cells, SK-Mel-28 melanoma cells, L929 mouse fibroblasts, and mouse monocyte/macrophage cells (J774A1).

However, conflicting results have been reported. For example, exposure to 5 nm TiO_2-NPs inhibited A549 cell proliferation and led to apoptosis and intracellular ROS production [43]. In another study 25 nm TiO_2-NPs showed greater toxicity than 60 nm TiO_2-NPs in A549 and 16HBE cells [44]. In addition, Simon-Deckers et al. as well as Zhu et al. reported that smaller TiO_2-NPs caused higher toxicity than bigger ones [45,46]. Therefore, there is no definitive conclusion about the effect of particle size on toxicity. Another example is that 50 nm TiO_2-NPs caused greater toxicity than the 6.3, 10, and 100 nm TiO_2-NPs [47]. Similarly, an interesting finding was that 25 nm TiO_2-NPs induced more cell death, higher LDH release, and ROS production than 5 and 100 nm TiO_2-NPs in mouse macrophages [48]. Therefore, toxic effect of TiO_2-NPs may be related to their structural characteristics as suggested by Zhang et al. [48]. More mechanistic studies are needed to clarify NP size impact on cytotoxicity.

Regarding the production of ROS, Jiang et al. [49] reported an S-shaped curve for ROS generation per unit surface area within a certain size range (4-195 nm) of TiO_2-NPs. Also, TiO_2-NPs below 10 nm or above 30 nm produced similar levels of ROS per surface area while a sharp increase was observed from 10 nm to 30 nm. ROS production was clearly observed in A549 cells in two studies [45,50] whatever the size, crystal phase and shape of TiO_2-NPs which were studied in conditions very similar to ours (same cellular model: A549 cells exposed to various types of

TiO_2-NPs, for 24h at 100 µg/mL). Especially, intracellular ROS production started as early as after 15 min of exposure to P25 [50]. However, in our study, TiO_2-NPs did not trigger the production of ROS whatever the size and surface area. This must be confirmed by a comprehensive study of the oxidative stress also including the assessment of anti-oxidant systems induction.

4.2 Shape effects

When comparing rod-shaped S3 and spherical P25 NPs, we observed that S3 NPs caused more cell death than P25 in co-culture suggesting an impact of NP shape on cell viability. However, NP shape had no impact on ROS production and did not seem to influence the pro-inflammatory response as in co-cultures P25 and S3 induced similar IL-8 and TNF-α productions. Only in A549 cells, P25 caused more IL-8 production than S3 but at the highest NP concentration.

A limited number of studies have considered how the shape of NPs impacts on their toxicity [20,51,52], and only few papers reported about a specific shape effect of TiO_2-NPs [53,54]. Gea et al. [53] investigated the cytotoxicity of TiO_2-NPs of three different shapes (bipyramids, rods, platelets) on human bronchial epithelial cells (BEAS-2B) in the presence or absence of light. They observed that in the presence of light, rod shaped TiO_2 were more cytotoxic than bipyramids and platelets, these latter showing a similar profile of toxicity. However, in the absence of light, platelets induced a higher cytotoxicity than bipyramids and rods. In an *in vivo* study [54], male Sprague-Dawley rats were exposed to sphere anatase/rutile P25, sphere pure anatase TiO_2, and nanobelts pure anatase TiO_2 by intratracheal instillation. Only nanobelts were able to induce inflammation *in vivo*. Studies using other NP types could be mentioned to illustrate the NP shape influence on cytotoxicity. For example, rod-shaped Fe_2O_3 NPs were found to produce much higher levels of lactate dehydrogenase (LDH) leakage, inflammatory response, and ROS production than sphere Fe_2O_3 NPs in RAW 264.7 [52]. On the contrary, Forest

et al. [20] reported that rod-shaped CeO_2 NPs produced more toxic effects in terms of LDH release and TNF-α production than octahedron or cubic CeO_2 NPs in RAW 264.7 cells.

On the other hand, some studies did not report any effect of NP shape on their cytotoxicity. For instance, Zhao et al. [55] did not find a significant difference in the toxicity of rod and sphere mesoporous silica NPs on human colorectal adenocarcinoma (Caco-2) cells.

The discrepancies described above can be explained by the fact that besides the shape of the NPs, NPs' interaction forces which are different for each type of particle may also affect biological responses, *e.g.* inter-particle Van der Waals forces of rod-shaped NPs are larger than those of spherical ones [56,57]. These forces define the ability of NP's cell internalization via phagocytosis [17,58]. Meng et al. [59] reported that the internalization of rod-shaped silica particles in A549 cells was much higher than that of spherical particles. This may explain why rod-shaped particles caused more cell death in our study. Moreover, when having different attractive forces (Van der Waals and others), the tendency to agglomerate in the suspension may also be different [60]. Therefore, it is also difficult to distinguish the shape effect from the agglomeration effect, since agglomeration always occurs in an aqueous system. Finally, due to different cell types, cell sensitivity, and phagocytic activity, it is difficult to compare studies from the literature.

4.3 Agglomeration effects

We compared the responses induced by S2 and P25 to determine the effect of agglomeration on toxicity because primary size, surface area, surface charge, and shape of the two particles were all similar, only their agglomeration state differed. When considering cell viability, highly agglomerated S2 NPs caused less cell death than less agglomerated P25 in both cell systems. Furthermore, IL-8 production was enhanced in the presence of less agglomerated NPs compared to that induced by highly agglomerated NPs in A549 but only at the highest NP

concentration. In addition, agglomeration did not affect IL-8 and TNF-α production in co-cultures and had no impact on ROS production.

Magdolenova et al. [61] reported that the highly agglomerated TiO_2-NPs decreased the proliferation activity in Cos-1 monkey kidney fibroblast-like cell line and EUE human embryonic epithelial cells compared to well-dispersed NPs. Large agglomerates of TiO_2-NPs caused DNA damage whereas small agglomerates did not. Another study reported that [62] in comparison to large A14 TiO_2-NP agglomerates, P25 and A60 TiO_2-NPs that exhibit small and soft agglomerates were more efficiently taken up by the A549 cells, generated more intracellular oxidative stress and induced more potent interleukin-8 (IL-8) and monocyte chemotactic protein 1 (MCP-1) pro-inflammatory response.

There are few *in vivo* studies in the literature which investigated the agglomeration impact of NPs on lung diseases. Noël et al. [63] exposed male CDF (F344)/CrlBR rats to aerosolized nano-TiO_2. In groups exposed to large agglomerates (>100 nm), an increase in the number of neutrophils, an indicator of lung inflammation was observed. However, no increase in other inflammation markers (IL-1α, Il-6, and TNF-α production) was observed. Exposure to small agglomerates (<100 nm) caused more cell death and ROS production than large agglomerates. Although these results are in agreement with ours, at least regarding cell viability, it is difficult to compare *in vivo* and *in vitro* studies because of a different agglomeration status of NPs that can occur *in vitro* (in culture medium) and *in vivo* in lung fluids. The protein corona forming around the NPs may also have a strong impact on agglomeration and on the subsequent cell/NP interactions [64].

4.4 Surface charge effects

When the impact of NP surface charge on cell viability was examined, it was observed that positively charged S4 NPs (APTES-functionalized) caused slightly more cell loss than S2, their

non-functionalized, negatively charged counterparts. However, they exhibited a similar profile of pro-inflammatory response and oxidative stress suggesting no impact of this functionalization on pro-inflammatory response and oxidative stress. Since it is well documented that positively charged NPs have high affinity for negatively charged cell membrane protein [65], it is more likely to have a destructive effect on cell membranes.

In a study [66], TiO_2-NPs bearing -OH, -NH_2, or –COOH surface groups, were evaluated for their effect on several cancer cell and control cell cytotoxicity. Specifically, -NH_2 and -OH groups exhibited significantly higher toxicity than -COOH on Lewis lung carcinoma (LLC), JHU prostate cancer cells. Some studies on other APTES functionalized NPs, for instance, the cytotoxicity of APTES functionalized mesoporous and nonporous silica NPs was investigated on RAW 264.7 macrophages [67]. They both induced very low levels of toxicity. Also, these particles did not cause any ROS production, similar to our results. Chavez et al. [68] reported that APTES functionalized luminescent upconversion NPs were found non-cytotoxic on HeLa and DLD-1 human colorectal adenocarcinoma cells. Petushov et al. [69] showed that 30 nm APTES functionalized silicalite NPs did not significantly change LDH release activity in HEK293 embryonic kidney cells and in RAW264.7 cells.

Beside the observation of the impact of the NPs physicochemical properties on their toxicity, another main finding of this study was that the co-culture model seemed more sensitive to the adverse effects of TiO_2-NPs than the monoculture model. It may be due to different uptake levels of NPs in monoculture and co-culture cells. Co-culture cells may show a stronger barrier compared to monoculture due to intercellular bonds and interactions. In a tetra-culture model consisting of A549 + THP-1 + HMC-1 + EAhy926 cells, only phagocytic THP-1 cells have been shown to internalize 50 nm silica particles [70]. Due to cell interaction through cytokines and chemokines, uptake in one cell type may affect the reaction of the other cell types in the

same culture. This can lead to differences in the uptake mechanisms of NPs compared to monoculture. However, in our study, further investigations are needed to support this hypothesis. On the other hand, the fact that co-culture is more sensitive to the toxic effects of NPs may result from different behaviors of cells in the co-culture. Data showed that when co-cultured with A549 cells, THP-1-derived macrophages (M0) differentiated towards the M1- and M2-macrophage phenotype. Therefore the co-culture of THP-1-derived macrophages with A549 leads to the release of higher levels of pro-inflammatory cytokines compared to levels observed in the medium of THP1-derived macrophages [71]. In this case, it has been reported a strong protection of A549 cells provided by THP-1 cells against toxic agents in co-culture. However, in order to mimic aerosol accumulation in the air space of the lung, direct cell culture may have some limitations given the weak interactions of the cells [72]. Also, different proliferation rates of the co-cultured cells may present a problem and limit the use of co-cultures. The multiple cell cultures represent an improvement compared with single cell cultures and more closely resemble the *in vivo* situation, yet they are still limited to the cells investigated. Thus, co-culture cell model may be considered as essential for developing a predictive *in vitro* model of the lung.

5. Conclusion

As reported in Table 3, the main effects observed in this study were an impact of TiO_2-NP size/SSA, shape, agglomeration state, and surface functionalization/charge (APTES) on cell viability in co-cultures. This model seems more sensitive than A549 monocultures. The same features seemed to have an impact on the pro-inflammatory response but only in A549 cells cultivated alone and only at the highest NP concentration. No impact was observed on ROS production. The effect on toxicity was higher in bigger sized, less agglomerated particles, rod-shaped and positively charged particles. Although further investigations are needed, the present

study contributes to a better characterization of TiO_2-NP toxicity by the systematic evaluation of their adverse effects on human lung cell lines in relation to their physicochemical properties. Moreover, such results could open promising perspectives, especially in the context of a safer-by-design approach.

Funding

This research did not receive any specific grant from funding agencies in the public, commercial, or not-for-profit sectors.

Supporting Information

XRD pattern of the TiO_2-NPs.

References

(1) Fujishima, A.; Rao, T. N.; Tryk, D. A. Titanium Dioxide Photocatalysis. *J. Photochem. Photobiol. C Photochem. Rev.* **2000**, *1* (1), 1–21. https://doi.org/10.1016/S1389-5567(00)00002-2.

(2) Chen, X.; Selloni, A. Introduction: Titanium Dioxide (TiO2) Nanomaterials. *Chem. Rev.* **2014**, *114* (19), 9281–9282. https://doi.org/10.1021/cr500422r.

(3) U.S. Geological Survey. Mineral Commodity Summaries 2015 Mineral Commodity Summaries 2015. *US Geol. Surv.* **2015**, 196. https://doi.org/10.3133/70140094.

(4) Weir, A.; Westerhoff, P.; Fabricius, L.; Hristovski, K.; Von Goetz, N. Titanium Dioxide Nanoparticles in Food and Personal Care Products. *Environ. Sci. Technol.* **2012**, *46* (4), 2242–2250. https://doi.org/10.1021/es204168d.

(5) Wang, Y.; He, Y.; Lai, Q.; Fan, M. Review of the Progress in Preparing Nano TiO2: An Important Environmental Engineering Material. *Journal of Environmental Sciences*

(China). Chinese Academy of Sciences November 1, **2014**, pp 2139–2177. https://doi.org/10.1016/j.jes.2014.09.023.

(6) Piccinno, F.; Gottschalk, F.; Seeger, S.; Nowack, B. Industrial Production Quantities and Uses of Ten Engineered Nanomaterials in Europe and the World. *J. Nanoparticle Res.* **2012**, *14* (9).

(7) Shi, H.; Magaye, R.; Castranova, V.; Zhao, J. Titanium Dioxide Nanoparticles: A Review of Current Toxicological Data. *Part. Fibre Toxicol.* **2013**, *10* (1).

(8) Grande, F.; Tucci, P. Titanium Dioxide Nanoparticles: A Risk for Human Health? *Mini-Reviews Med. Chem.* **2016**, *16* (9), 762–769. https://doi.org/10.2174/1389557516666160321114341.

(9) Baranowska-Wójcik, E.; Szwajgier, D.; Oleszczuk, P.; Winiarska-Mieczan, A. Effects of Titanium Dioxide Nanoparticles Exposure on Human Health—a Review. *Biol. Trace Elem. Res.* **2020**, *193* (1), 118–129. https://doi.org/10.1007/s12011-019-01706-6.

(10) Albanese, A.; Tang, P. S.; Chan, W. C. W. The Effect of Nanoparticle Size, Shape, and Surface Chemistry on Biological Systems. *Annu. Rev. Biomed. Eng.* **2012**, *14* (1), 1–16. https://doi.org/10.1146/annurev-bioeng-071811-150124.

(11) Oberdörster, G.; Oberdörster, E.; Oberdörster, J. Nanotoxicology: An Emerging Discipline Evolving from Studies of Ultrafine Particles. *Environ. Health Perspect.* **2005**, *113* (7), 823–839. https://doi.org/10.1289/ehp.7339.

(12) Oberdörster, G.; Ferin, J.; Lehnert, B. E. Correlation between Particle Size, in Vivo Particle Persistence, and Lung Injury. *Environ. Health Perspect.* **1994**, *102 Suppl 5* (Suppl 5), 173–179. https://doi.org/10.1289/ehp.102-1567252.

(13) Braakhuis, H. M.; Gosens, I.; Krystek, P.; Boere, J. A.; Cassee, F. R.; Fokkens, P. H.; Post, J. A.; van Loveren, H.; Park, M. V. Particle Size Dependent Deposition and Pulmonary Inflammation after Short-Term Inhalation of Silver Nanoparticles. *Part.*

Fibre Toxicol. **2014**, *11* (1), 49. https://doi.org/10.1186/s12989-014-0049-1.

(14) Kuehl, P. J.; Anderson, T. L.; Candelaria, G.; Gershman, B.; Harlin, K.; Hesterman, J. Y.; Holmes, T.; Hoppin, J.; Lackas, C.; Norenberg, J. P.; Yu, H.; McDonald, J. D. Regional Particle Size Dependent Deposition of Inhaled Aerosols in Rats and Mice. *Inhal. Toxicol.* **2012**, *24* (1), 27–35. https://doi.org/10.3109/08958378.2011.632787.

(15) Asgharian, B.; Price, O. T. Deposition of Ultrafine (NANO) Particles in the Human Lung. *Inhal. Toxicol.* **2007**, *19* (13), 1045–1054. https://doi.org/10.1080/08958370701626501.

(16) Verma, A.; Stellacci, F. Effect of Surface Properties on Nanoparticleâ€“Cell Interactions. *Small* **2010**, *6* (1), 12–21. https://doi.org/10.1002/smll.200901158.

(17) Champion, J. A.; Mitragotri, S. Role of Target Geometry in Phagocytosis. *Proc. Natl. Acad. Sci. U. S. A.* **2006**, *103* (13), 4930–4934. https://doi.org/10.1073/pnas.0600997103.

(18) Park, S.; Lee, Y. K.; Jung, M.; Kim, K. H.; Chung, N.; Ahn, E.-K.; Lim, Y.; Lee, K.-H. Cellular Toxicity of Various Inhalable Metal Nanoparticles on Human Alveolar Epithelial Cells. *Inhal. Toxicol.* **2007**, *19* (sup1), 59–65. https://doi.org/10.1080/08958370701493282.

(19) Hsiao, I.-L.; Huang, Y.-J. Effects of Various Physicochemical Characteristics on the Toxicities of ZnO and TiO2 Nanoparticles toward Human Lung Epithelial Cells. *Sci. Total Environ.* **2011**, *409* (7), 1219–1228. https://doi.org/10.1016/j.scitotenv.2010.12.033.

(20) Forest, V.; Leclerc, L.; Hochepied, J.-F.; Trouvé, A.; Sarry, G.; Pourchez, J. Impact of Cerium Oxide Nanoparticles Shape on Their in Vitro Cellular Toxicity. *Toxicol. Vitr.* **2017**, *38*, 136–141. https://doi.org/10.1016/j.tiv.2016.09.022.

(21) IARC. IARC Monographs on the Evaluation of Carcinogenic Risks to Humans Carbon

Black, Titanium Dioxide, and Talc. *IARC* **2006**, *93*, 193–412. https://doi.org/10.1136/jcp.48.7.691-a.

(22) Fadeel, B. Nanosafety: Towards Safer Design of Nanomedicines. *J. Intern. Med.* **2013**, *274* (6), 578–580. https://doi.org/10.1111/joim.12137.

(23) Geraci, C.; Heidel, D.; Sayes, C.; Hodson, L.; Schulte, P.; Eastlake, A.; Brenner, S. Perspectives on the Design of Safer Nanomaterials and Manufacturing Processes. *J. Nanoparticle Res.* **2015**, *17* (9), 1–13. https://doi.org/10.1007/s11051-015-3152-9.

(24) Shin, S. W.; Song, I. H.; Um, S. H. Role of Physicochemical Properties in Nanoparticle Toxicity. *Nanomater. (Basel, Switzerland)* **2015**, *5* (3), 1351–1365. https://doi.org/10.3390/nano5031351.

(25) Iavicoli, I.; Leso, V.; Bergamaschi, A. Toxicological Effects of Titanium Dioxide Nanoparticles: A Review of in Vivo Studies. *Journal of Nanomaterials*. 2012. https://doi.org/10.1155/2012/964381.

(26) Chen, D. W.; Shi, J. E.; Yan, J. C.; Wang, Y. H.; Yan, F. C.; Shang, S. X.; Xue, J. Controllable Synthesis of Titania Nanocrystals with Different Morphologies and Application to the Degradation of Phenol. *Chem. Res. Chinese Univ.* **2008**, *24* (3), 362–366. https://doi.org/10.1016/S1005-9040(08)60076-8.

(27) Zhao, J.; Milanova, M.; Warmoeskerken, M. M. C. G.; Dutschk, V. Surface Modification of TiO2 Nanoparticles with Silane Coupling Agents. *Colloids Surfaces A Physicochem. Eng. Asp.* **2012**, *413*, 273–279. https://doi.org/10.1016/j.colsurfa.2011.11.033.

(28) Brunauer, S.; Emmett, P. H.; Teller, E. Adsorption of Gases in Multimolecular Layers. *J. Am. Chem. Soc.* **1938**, *60* (2), 309–319. https://doi.org/10.1021/ja01269a023.

(29) Wang, Z.; Ni, Z.; Qiu, D.; Chen, T.; Tao, G.; Yang, P. Determination of Metal Impurities in Titanium Dioxide Using Slurry Sample Introduction by Axial Viewing Inductively Coupled Plasma Optical Emission Spectrometry. *J. Anal. At. Spectrom.* **2004**, *19* (2),

273. https://doi.org/10.1039/b307495a.

(30) Wang, S.; Yu, H.; Wickliffe, J. K. Limitation of the MTT and XTT Assays for Measuring Cell Viability Due to Superoxide Formation Induced by Nano-Scale TiO 2. *Toxicol. Vitr.* **2011**, *25* (8), 2147–2151. https://doi.org/10.1016/j.tiv.2011.07.007.

(31) Holder, A. L.; Goth-Goldstein, R.; Lucas, D.; Koshland, C. P. Particle-Induced Artifacts in the MTT and LDH Viability Assays. *Chem. Res. Toxicol.* **2012**. https://doi.org/10.1021/tx3001708.

(32) Drumm, K.; Attia, D. I.; Kannt, S.; Micke, P.; Buhl, R.; Kienast, K. Soot-Exposed Mononuclear Cells Increase Inflammatory Cytokine MRNA Expression and Protein Secretion in Cocultured Bronchial Epithelial Cells. *Respiration* **2000**, *67* (3), 291–297. https://doi.org/10.1159/000029513.

(33) Holownia, A.; Wielgat, P.; Kwolek, A.; Jackowski, K.; Braszko, J. J. Crosstalk between Co-Cultured A549 Cells and Thp1 Cells Exposed to Cigarette Smoke. *Adv. Exp. Med. Biol.* **2015**, *858*, 47–55. https://doi.org/10.1007/5584_2015_112.

(34) Dehai, C.; Bo, P.; Qiang, T.; Lihua, S.; Fang, L.; Shi, J.; Jingyan, C.; Yan, Y.; Guangbin, W.; Zhenjun, Y. Enhanced Invasion of Lung Adenocarcinoma Cells after Co-Culture with THP-1-Derived Macrophages via the Induction of EMT by IL-6. *Immunol. Lett.* **2014**, *160* (1), 1–10. https://doi.org/10.1016/j.imlet.2014.03.004.

(35) Uboldi, C.; Urbán, P.; Gilliland, D.; Bajak, E.; Valsami-Jones, E.; Ponti, J.; Rossi, F. Role of the Crystalline Form of Titanium Dioxide Nanoparticles: Rutile, and Not Anatase, Induces Toxic Effects in Balb/3T3 Mouse Fibroblasts. *Toxicol. Vitr.* **2016**, *31*, 137–145. https://doi.org/10.1016/j.tiv.2015.11.005.

(36) Gerloff, K.; Fenoglio, I.; Carella, E.; Kolling, J.; Albrecht, C.; Boots, A. W.; Förster, I.; Schins, R. P. F. Distinctive Toxicity of TiO 2 Rutile/Anatase Mixed Phase Nanoparticles on Caco-2 Cells. *Chem. Res. Toxicol.* **2012**, *25* (3), 646–655.

https://doi.org/10.1021/tx200334k.

(37) Sayes, C. M.; Wahi, R.; Kurian, P. A.; Liu, Y.; West, J. L.; Ausman, K. D.; Warheit, D. B.; Colvin, V. L. Correlating Nanoscale Titania Structure with Toxicity: A Cytotoxicity and Inflammatory Response Study with Human Dermal Fibroblasts and Human Lung Epithelial Cells. *Toxicol. Sci.* **2006**, *92* (1), 174–185. https://doi.org/10.1093/toxsci/kfj197.

(38) Kraegeloh, A.; Suarez-Merino, B.; Sluijters, T.; Micheletti, C. Implementation of Safe-by-Design for Nanomaterial Development and Safe Innovation: Why We Need a Comprehensive Approach. *Nanomaterials* **2018**, *8* (4). https://doi.org/10.3390/nano8040239.

(39) Zhang, S.; Gao, H.; Bao, G. Physical Principles of Nanoparticle Cellular Endocytosis. *ACS Nano* **2015**, *9* (9), 8655–8671. https://doi.org/10.1021/acsnano.5b03184.

(40) Hoshyar, N.; Gray, S.; Han, H.; Bao, G. The Effect of Nanoparticle Size on *in Vivo* Pharmacokinetics and Cellular Interaction. *Nanomedicine* **2016**, *11* (6), 673–692. https://doi.org/10.2217/nnm.16.5.

(41) Yin, H.; Too, H. P.; Chow, G. M. The Effects of Particle Size and Surface Coating on the Cytotoxicity of Nickel Ferrite. *Biomaterials* **2005**, *26* (29), 5818–5826. https://doi.org/10.1016/j.biomaterials.2005.02.036.

(42) Pan, Y.; Neuss, S.; Leifert, A.; Fischler, M.; Wen, F.; Simon, U.; Schmid, G.; Brandau, W.; Jahnen-Dechent, W. Size-Dependent Cytotoxicity of Gold Nanoparticles. *Small* **2007**, *3* (11), 1941–1949. https://doi.org/10.1002/smll.200700378.

(43) Wang, Y.; Cui, H.; Zhou, J.; Li, F.; Wang, J.; Chen, M.; Liu, Q. Cytotoxicity, DNA Damage, and Apoptosis Induced by Titanium Dioxide Nanoparticles in Human Non-Small Cell Lung Cancer A549 Cells. *Environ. Sci. Pollut. Res.* **2015**, *22* (7), 5519–5530. https://doi.org/10.1007/s11356-014-3717-7.

(44) Ma, Y.; Guo, Y.; Wu, S.; Lv, Z.; Zhang, Q.; Ke, Y. Titanium Dioxide Nanoparticles Induce Size-Dependent Cytotoxicity and Genomic DNA Hypomethylation in Human Respiratory Cells. *RSC Adv.* **2017**, *7* (38), 23560–23572. https://doi.org/10.1039/c6ra28272e.

(45) Simon-Deckers, A.; Gouget, B.; Mayne-L'Hermite, M.; Herlin-Boime, N.; Reynaud, C.; Carrière, M. In Vitro Investigation of Oxide Nanoparticle and Carbon Nanotube Toxicity and Intracellular Accumulation in A549 Human Pneumocytes. *Toxicology* **2008**, *253* (1–3), 137–146. https://doi.org/10.1016/J.TOX.2008.09.007.

(46) Zhu, R. R.; Wang, S. L.; Chao, J.; Shi, D. L.; Zhang, R.; Sun, X. Y.; Yao, S. D. Bio-Effects of Nano-TiO2 on DNA and Cellular Ultrastructure with Different Polymorph and Size. *Mater. Sci. Eng. C* **2009**, *29* (3), 691–696. https://doi.org/10.1016/j.msec.2008.12.023.

(47) Braydich-Stolle, L. K.; Schaeublin, N. M.; Murdock, R. C.; Jiang, J.; Biswas, P.; Schlager, J. J.; Hussain, S. M. Crystal Structure Mediates Mode of Cell Death in TiO2 Nanotoxicity. *J. Nanoparticle Res.* **2009**, *11* (6), 1361–1374. https://doi.org/10.1007/s11051-008-9523-8.

(48) Zhang, J.; Song, W.; Guo, J.; Zhang, J.; Sun, Z.; Li, L.; Ding, F.; Gao, M. Cytotoxicity of Different Sized TiO2nanoparticles in Mouse Macrophages. *Toxicol. Ind. Health* **2013**, *29* (6), 523–533. https://doi.org/10.1177/0748233712442708.

(49) Jiang, J.; Oberdörster, G.; Elder, A.; Gelein, R.; Mercer, P.; Biswas, P. Does Nanoparticle Activity Depend upon Size and Crystal Phase? *Nanotoxicology* **2008**, *2* (1), 33–42. https://doi.org/10.1080/17435390701882478.

(50) Jugan, M. L.; Barillet, S.; Simon-Deckers, A.; Herlin-Boime, N.; Sauvaigo, S.; Douki, T.; Carriere, M. Titanium Dioxide Nanoparticles Exhibit Genotoxicity and Impair DNA Repair Activity in A549 Cells. *Nanotoxicology* **2012**, *6* (5), 501–513.

https://doi.org/10.3109/17435390.2011.587903.

(51) Wang, L.; Ai, W.; Zhai, Y.; Li, H.; Zhou, K.; Chen, H. Effects of Nano-CeO2 with Different Nanocrystal Morphologies on Cytotoxicity in HepG2 Cells. *Int. J. Environ. Res. Public Health* **2015**, *12* (9), 10806–10819. https://doi.org/10.3390/ijerph120910806.

(52) Lee, J. H.; Ju, J. E.; Kim, B. Il; Pak, P. J.; Choi, E.-K.; Lee, H.-S.; Chung, N. Rod-Shaped Iron Oxide Nanoparticles Are More Toxic than Sphere-Shaped Nanoparticles to Murine Macrophage Cells. *Environ. Toxicol. Chem.* **2014**, *33* (12), 2759–2766. https://doi.org/10.1002/etc.2735.

(53) Gea, M.; Bonetta, S.; Iannarelli, L.; Giovannozzi, A. M.; Maurino, V.; Bonetta, S.; Hodoroaba, V. D.; Armato, C.; Rossi, A. M.; Schilirò, T. Shape-Engineered Titanium Dioxide Nanoparticles (TiO 2 -NPs): Cytotoxicity and Genotoxicity in Bronchial Epithelial Cells. *Food Chem. Toxicol.* **2019**, *127*, 89–100. https://doi.org/10.1016/j.fct.2019.02.043.

(54) Silva, R. M.; TeeSy, C.; Franzi, L.; Weir, A.; Westerhoff, P.; Evans, J. E.; Pinkerton, K. E. Biological Response to Nano-Scale Titanium Dioxide (TiO_2): Role of Particle Dose, Shape, and Retention. *J. Toxicol. Environ. Heal. Part A* **2013**, *76* (16), 953–972. https://doi.org/10.1080/15287394.2013.826567.

(55) Zhao, Y.; Wang, Y.; Ran, F.; Cui, Y.; Liu, C.; Zhao, Q.; Gao, Y.; Wang, D.; Wang, S. A Comparison between Sphere and Rod Nanoparticles Regarding Their in Vivo Biological Behavior and Pharmacokinetics. *Sci. Rep.* **2017**, *7* (1), 4131. https://doi.org/10.1038/s41598-017-03834-2.

(56) Brown, S. C.; Kamal, M.; Nasreen, N.; Baumuratov, A.; Sharma, P.; Antony, V. B.; Moudgil, B. M. Influence of Shape, Adhension and Simulated Lung Mechanics on Amorphous Silica Nanoparticle Toxicity. *Adv. Powder Technol.* **2007**, *18* (1), 69–79.

https://doi.org/10.1163/156855207779768214.

(57) Vold, M. J. Van Der Waals' Attraction between Anisometric Particles. *J. Colloid Sci.* **1954**, *9* (5), 451–459. https://doi.org/10.1016/0095-8522(54)90032-X.

(58) Yameen, B.; Choi, W. Il; Vilos, C.; Swami, A.; Shi, J.; Farokhzad, O. C. Insight into Nanoparticle Cellular Uptake and Intracellular Targeting. *Journal of Controlled Release*. Elsevier B.V. September 28, 2014, pp 485–499. https://doi.org/10.1016/j.jconrel.2014.06.038.

(59) Meng, H.; Yang, S.; Li, Z.; Xia, T.; Chen, J.; Ji, Z.; Zhang, H.; Wang, X.; Lin, S.; Huang, C.; Zhou, Z. H.; Zink, J. I.; Nel, A. E. Aspect Ratio Determines the Quantity of Mesoporous Silica Nanoparticle Uptake by a Small Gtpase-Dependent Macropinocytosis Mechanism. *ACS Nano* **2011**, *5* (6), 4434–4447. https://doi.org/10.1021/nn103344k.

(60) Powers, K. W.; Palazuelos, M.; Moudgil, B. M.; Roberts, S. M. Characterization of the Size, Shape, and State of Dispersion of Nanoparticles for Toxicological Studies. *Nanotoxicology* **2007**, *1* (1), 42–51. https://doi.org/10.1080/17435390701314902.

(61) Magdolenova, Z.; Bilaničová, D.; Pojana, G.; Fjellsbø, L. M.; Hudecova, A.; Hasplova, K.; Marcomini, A.; Dusinska, M. Impact of Agglomeration and Different Dispersions of Titanium Dioxide Nanoparticles on the Human Related in Vitro Cytotoxicity and Genotoxicity. *J. Environ. Monit.* **2012**, *14* (2), 455. https://doi.org/10.1039/c2em10746e.

(62) Andersson, P. O.; Lejon, C.; Ekstrand-Hammarström, B.; Akfur, C.; Ahlinder, L.; Bucht, A.; Österlund, L. Polymorph- and Size-Dependent Uptake and Toxicity of TiO 2 Nanoparticles in Living Lung Epithelial Cells. *Small* **2011**, *7* (4), 514–523. https://doi.org/10.1002/smll.201001832.

(63) Noël, A.; Maghni, K.; Cloutier, Y.; Dion, C.; Wilkinson, K. J.; Hallé, S.; Tardif, R.; Truchon, G. Effects of Inhaled Nano-TiO2 Aerosols Showing Two Distinct

Agglomeration States on Rat Lungs. *Toxicol. Lett.* **2012**, *214* (2), 109–119. https://doi.org/10.1016/J.TOXLET.2012.08.019.

(64) Forest, V.; Cottier, M.; Pourchez, J. Electrostatic Interactions Favor the Binding of Positive Nanoparticles on Cells: A Reductive Theory. *Nano Today* **2015**, *10* (6), 677–680. https://doi.org/10.1016/J.NANTOD.2015.07.002.

(65) Wilhelm, C.; Billotey, C.; Roger, J.; Pons, J. N.; Bacri, J. C.; Gazeau, F. Intracellular Uptake of Anionic Superparamagnetic Nanoparticles as a Function of Their Surface Coating. *Biomaterials* **2003**, *24* (6), 1001–1011. https://doi.org/10.1016/S0142-9612(02)00440-4.

(66) Thevenot, P.; Cho, J.; Wavhal, D.; Timmons, R. B.; Tang, L. Surface Chemistry Influences Cancer Killing Effect of TiO2 Nanoparticles. *Nanomedicine Nanotechnology, Biol. Med.* **2008**, *4* (3), 226–236. https://doi.org/10.1016/j.nano.2008.04.001.

(67) Lehman, S. E.; Morris, A. S.; Mueller, P. S.; Salem, A. K.; Grassian, V. H.; Larsen, S. C. Silica Nanoparticle-Generated ROS as a Predictor of Cellular Toxicity: Mechanistic Insights and Safety by Design. *Environ. Sci. Nano* **2016**, *3* (1), 56–66. https://doi.org/10.1039/C5EN00179J.

(68) Chavez, D. H.; Juarez-Moreno, K.; Hirata, G. A. Aminosilane Functionalization and Cytotoxicity Effects of Upconversion Nanoparticles Y2O3 and Gd2O3 Co-Doped with Yb3+and Er3. *Nanobiomedicine* **2016**, *3*, 1. https://doi.org/10.5772/62252.

(69) Petushkov, A.; Intra, J.; Graham, J. B.; Larsen, S. C.; Salem, A. K. Effect of Crystal Size and Surface Functionalization on the Cytotoxicity of Silicalite-1 Nanoparticles. *Chem. Res. Toxicol.* **2009**, *22* (7), 1359–1368. https://doi.org/10.1021/tx900153k.

(70) Klein, S. G.; Serchi, T.; Hoffmann, L.; Blömeke, B.; Gutleb, A. C. An Improved 3D Tetraculture System Mimicking the Cellular Organisation at the Alveolar Barrier to Study the Potential Toxic Effects of Particles on the Lung. *Part. Fibre Toxicol.* **2013**, *10*

(1). https://doi.org/10.1186/1743-8977-10-31.

(71) Dehai, C.; Bo, P.; Qiang, T.; Lihua, S.; Fang, L.; Shi, J.; Jingyan, C.; Yan, Y.; Guangbin, W.; Zhenjun, Y. Enhanced Invasion of Lung Adenocarcinoma Cells after Co-Culture with THP-1-Derived Macrophages via the Induction of EMT by IL-6. *Immunol. Lett.* **2014**, *160* (1), 1–10. https://doi.org/10.1016/j.imlet.2014.03.004.

(72) Rothen-Rutishauser, B. M.; Kiama, S. C.; Gehr, P. A Three-Dimensional Cellular Model of the Human Respiratory Tract to Study the Interaction with Particles. *Am. J. Respir. Cell Mol. Biol.* **2005**, *32* (4), 281–289. https://doi.org/10.1165/rcmb.2004-0187OC.

Supporting Information

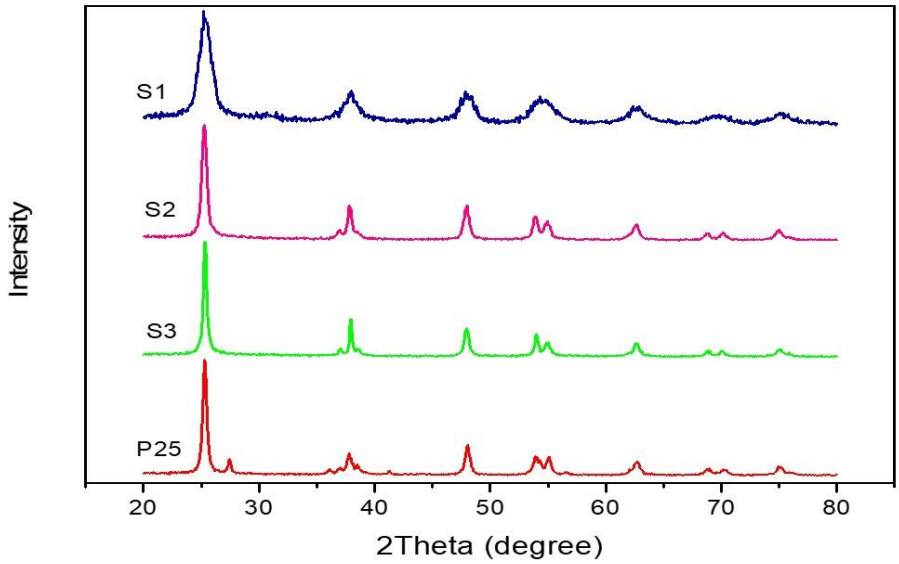

Supplementary figure 1: XRD patterns of TiO_2- NPs.